Construction and Building Materials 425 (2024) 136088

Contents lists available at ScienceDirect

Construction and Building Materials

journal homepage: www.elsevier.com/locate/conbuildmat

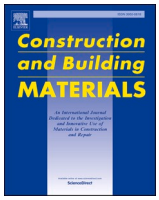

Enhancing fire resistance of masonry structures: The potential of ultra high performance concrete (UHPC)

L. Estevan [a,*], B. Torres [a], F.J. Baeza [a], V. Gattulli [b], S. Ivorra [a]

[a] DIC - Department of Civil Engineering, University of Alicante, P.O. Box 99, Alicante 03080, Spain
[b] DISG - Department of Structural and Geotechnical Engineering, Sapienza University of Rome, Rome 00184, Italy

ARTICLE INFO

Keywords:
UHPC
Masonry
Bond
Confinement
Shear strength
High temperature

ABSTRACT

The potential of ultra high performance concrete (UHPC) for strengthening masonry structures is evaluated in this work, both under normal service conditions and after exposure to high temperatures, as a significant gap has been identified on this topic at the present time. The mechanical properties of UHPC exposed up to 800 °C are analyzed by means of destructive and non-destructive tests, and the UHPC-to-masonry bond capacity is tested, depending on temperature and substrate preparation. The strengthening of masonry columns by confinement is studied, proving that UHPC jackets can double the compressive strength and provide ductility, even after exposure to high temperatures. Strengthening of masonry walls to in-plane loads is also evaluated, finding that UHPC layers can increase the shear strength and prevent brittle failures. Experimental results are compared with the predictions of theoretical models from some design guides, slightly adapted to the context of this research, obtaining a good degree of accuracy.

1. Introduction

The maintenance and preservation of masonry structures is a challenge for research in the field of structural engineering. These constructions are often considered to be outstanding architectural achievements in the cultural heritage and symbolic icons that embody past ages. In other cases, they are simply modest buildings in which millions of people live all over the world. In spite of their long-lasting character, masonry structures can also be vulnerable to threats such as earthquakes [1–4] or fire [5,6], which has given rise to a continuous search for innovative and scientifically solid solutions to improve their behavior under these extraordinary situations.

In this context, the most widely used strengthening methods at the present time are based mainly on textile reinforced mortars (TRM), thanks to the possibilities offered by this new generation of composites [7]. The wide-ranging research carried out in recent years has shown TRM to be highly efficient in improving the mechanical capacity of walls under monotonic [8–11] or cyclic loads [12–14], column confinement [15–17], and arches or vaults strengthening [18–20], among other applications. However, the effectiveness of these materials is limited in situations of high temperatures or fire scenarios [21]. At present, studies on TRM subjected to high temperatures are scarce and are basically limited to the analysis of the loss of mechanical properties by means of tensile coupons tests [22–25], or the evaluation of TRM-to-masonry bond capacity [26–29]. The main conclusions of these works reveal that the integrity of TRM can be seriously compromised by temperatures over 400 °C, even though these materials are often considered to be fire-resistant due to the incombustible nature of their inorganic matrices. In addition, thermal strain cracking can also affect the TRM-to-masonry bond even at lower temperatures, as evidenced by the changes in the failure mode of single-lap shear tests [29]. Nevertheless, regarding the behavior of masonry structures strengthened with TRM under high temperatures, this topic still remains practically unexplored, except for some papers published by the authors of the present work on walls tested under diagonal compression [30], or under in-plane cyclical loads [31].

The incompatibility of TRM with high temperatures requires a re-evaluation of the conventional strengthening strategies and favors the exploration for alternative materials able to withstand extreme fire conditions. In this context, ultra high performance concrete (UHPC), acclaimed for its exceptionally mechanical properties and durability [32–34], has emerged as a potential solution. UHPC is an advanced cementitious material with high compressive strength (above 120 MPa), usually reinforced with fibers that provide ductility under tension. The

* Corresponding author.
E-mail address: luis.estevan@ua.es (L. Estevan).

https://doi.org/10.1016/j.conbuildmat.2024.136088
Received 1 February 2024; Received in revised form 28 March 2024; Accepted 29 March 2024

strengthening capacity of UHPC has recently attracted the attention of the scientific community, focusing mainly on concrete structures, due to its ability to increase the flexural strength of beams and slabs [35,36], or improve the behavior of compressed columns by confinement [37–39]. However, the use of this material for retrofitting masonry members has hardly been explored to date. Among the few works available, it is worth mentioning an experimental study with walls strengthened on one side only and tested under in-plane cyclic loads [40]. The results reveal that the UHPC layer can improve the shear strength of the wall by 193%, cracking load by 127% and ultimate deformation by 109%. In addition, applied on a damaged wall, UHPC can fill cracks and damaged areas, and produce almost the same effect. In other study with square masonry columns under eccentric compressive loads [41], it is found that the peak load with a 30 mm thick UHPC jacket is increased by about 104%. In addition, the confined columns exhibit an excellent performance in the post-peak phase, in contrast to the brittle failures obtained in case of unconfined specimens. The results of these studies suggest that UHPC can be an efficient solution to increase the strength of masonry structures and provide them with ductility, in a simple easy-to-apply process. On the other hand, the effectiveness of UHPC reinforcements largely depends on their bond capacity, a property that has been analyzed for normal strength concrete [42–44], but hardly ever for stone or masonry substrates [45]. From these studies, it should be emphasized that UHPC usually exhibits good bonding on these surfaces, although the effectiveness of the reinforcement can mainly depend on the roughness or moisture content of the substrate.

Regarding the behavior of UHPC subjected to high temperatures, and from the point of view of the objectives of this research, some works analyzing the loss of mechanical properties of the material after exposure up to 700 - 800 °C are particularly relevant [46–51]. In general terms, the results show that UHPC partially retains its mechanical properties up to 500 - 600 °C, although it undergoes a strong degradation at higher temperatures. Consequently, it can be concluded that, compared with systems based on TRM, UHPC can offer an alternative strengthening solution with an interesting potential under high temperatures or fire scenarios.

After analyzing the state of the art in this area, and as a summary of what has been exposed in the preceding paragraphs, two fundamental conclusions should be highlighted: (i) UHPC strengthening of masonry structures is still a topic that remains largely unexplored and few studies have been made on the subject; and (ii) the particular case of UHPC reinforcements under high temperatures has not been investigated to date and no scientific paper has been found in the literature. Therefore, it is considered interesting to obtain experimental data to add to the present state of knowledge in this field, for which a four-phase research is planned. Firstly, the evolution of the mechanical properties of UHPC at temperatures of 20, 200, 400, 600 and 800 °C is analyzed, including compressive, flexural and tensile strength by means of destructive tests, and dynamic modulus of elasticity by non-destructive testing. Secondly, the bond capacity of UHPC on masonry substrates at temperatures of up to 600 °C is evaluated (it was found that after 800 °C the material suffered a strong degradation and completely lost its mechanical capacity). Since the effectiveness of the reinforcement can largely depend on the surface preparation, specimens with flush or raked joints were designed to simulate two situations commonly found in case of retrofitting the walls of a real building. Thirdly, the UHPC strengthening capacity for masonry members is studied, specifically the confinement of square cross-section columns and the increase of shear strength of panels subjected to in-plane loads. These tests were carried out at room temperature and after exposure to 600 °C in order to reproduce, under controlled laboratory conditions, possible fire scenarios to which these structural elements could be exposed. Finally, the experimental results are compared with the predictions of some design guides. At the present time, no standards are available for the strengthening of masonry structures with UHPC, so in this study the main reference guides published for TRM are adopted, specifically the American ACI 549.6R-20 [52] and the Italian CNR-DT 215/2018 [53]. One of the main novelties of this work is precisely to examine whether the theoretical models proposed by these guides could be used satisfactorily for the hypotheses proposed in this research, in spite of not being specifically formulated for masonry strengthened with UHPC, either under normal service conditions or after exposure to high temperatures.

2. Materials and methods

This section describes the properties of the materials, both the UHPC and the components of the masonry members, by means of destructive and non-destructive tests. On the other hand, the experimental methods to determine the tensile strength of UHPC, and the UHPC-to-masonry bond capacity (with two different surface treatments) are detailed. Both properties are crucial from the point of view of the objectives of this research. Finally, the experimental campaigns designed to study the potential of UHPC for masonry strengthening are described: confinement of columns and shear strengthening of masonry walls. Tests were performed at room temperature and after exposure up to 800 °C.

2.1. Properties of materials

The UHPC used in this research was provided by Mapei under the commercial designation “Planitop HPC”, which complies with the requirements of EN 1504–3:2005 [54] for R4-class structural mortars, as stated by the supplier. It is a ready-mixed free-flowing mortar made from two components: component A (made from high-strength cement, selected aggregates and special additives), and component B (stiff steel fibers). The mixing ratio, as specified by the manufacturer, is as follows: 100 parts by weight of component A, 6.5 parts by weight of component B, and 11.5 to 12.5 parts of water. This dosage results in a water/cement ratio of approximately 0.2. The main mechanical properties of the UHPC used, according to the data provided by the supplier, are as follows: density = 2450 kg/m^3; compressive strength = 130 MPa (after 28 days); compressive modulus of elasticity = 37 GPa (after 28 days); shear strength and slip resistance on concrete substrate with roughened surface $\geq$ 3.5 MPa; tensile strength at limit of proportionality, typical value = 7.2 MPa. Fig. 1 shows a view of the fibers used in the production of the UHPC. These fibers, 13 mm in length and 0.21 mm in diameter, are made of steel with a tensile strength of 2750 MPa and elongation at failure between 1.5 and 3%, as specified by the supplier.

The mechanical properties of the UHPC were determined

Fig. 1. Detail of the steel fibers used in the production of the UHPC.

experimentally, both at room temperature and after exposure to 200, 400, 600 and 800 °C, and the results are presented and discussed in detail in Section 3. For this purpose, 15 specimens of 160×40×40 mm^3 were prepared and tested in flexure and compression according to EN 1015–11:2019 [55], in series of three samples for each temperature level. A programmable electric oven was used, with an increasing heating curve of 10 °C/min until reaching the target temperature, which was kept constant for one hour. The specimens were stored for an additional 24 hours inside the switched-off oven until reaching the laboratory room temperature.

Regarding the masonry elements, solid fired clay bricks of dimensions 230×110×50 mm^3 were used, with a density of 1550 kg/m^3 and a compressive strength of 15 MPa, as declared by the manufacturer. New bricks supplied by a local brick factory were used to simulate traditional masonry, specifically columns and walls formed by two brick leaves in stretched bond, as specified in more detail in Sections 2.5 and 2.6. For the bed-joint mortar, a natural hydraulic lime mortar with pozzolan was used, with a density of 2000 kg/m^3 and a minimum compressive strength of 7.5 MPa, according to the data provided by the supplier. Both materials have been used in previous works developed by some of the authors of this research, and their properties have been experimentally characterized both at room temperature and after exposure up to 600 °C [29,30]. Table 1 summarizes the main results obtained, as reported in these papers. As can be seen, the bricks retain their mechanical properties relatively intact, while the bed-joint mortar seems to be much more damaged by the effect of high temperatures, with reductions of about 30% (in compression) and 60% (in bending), after exposure to 600 °C. On the other hand, it has been found in previous studies that exposure to high temperatures could reduce the mechanical capacity of masonry elements, mainly as a consequence of the bonding loss at the brick-mortar interface and the cracking of the member [31].

In addition, it is considered appropriate to highlight the curing periods adopted for each material. From previous research developed by some of the authors of this work [13,29–31], and following the recommendations from suppliers, the hydraulic lime mortar requires a 90-day curing period, while UHPC reaches full performance after 28 days. Consequently, the masonry members produced for this study were maintained for a minimum period of 90 days before applying the UHPC, to avoid affecting the natural development of the lime mortar strength. After UHPC application, an additional curing period of 28 days was scheduled to ensure full capacity of the reinforcements.

2.2. UHPC tensile strength test

From the point of view of the objectives of this study, one of the most important mechanical properties of UHPC is its tensile strength. For this purpose, 15 coupons of 500×100×10 mm^3 were produced in individual molds, which were kept in ambient laboratory conditions for 28 days, covered with a polyethylene sheet to preserve humidity. After this period, the samples were arranged in series of three specimens and subjected to the same temperature levels specified in Section 2.1, following the same heating procedure. The ends of the coupons were subsequently reinforced with FRP (quadriaxial glass fiber fabric and epoxy resin), 120 mm long on both sides, in order to improve the grip conditions with the press plates and prevent the failure of the samples in these areas.

The specimens were tested under uniaxial tensile following the recommendations of the AC434 [56] and RILEM TC 232-TDT [57] guidelines, and according to previous tests on TRM coupons exposed to high temperatures [24]. The tests were performed in an electric press equipped with a 50 kN load cell and the gripping device was designed to allow the free rotation of the specimen at both ends, in order to correct possible eccentricity or centering errors. The tests were carried out under displacement control at a constant rate of 0.2 mm/min. Two linear variable displacement transducers (LVTD) placed on both sides of the specimens were used to register the elongations, connected to an HBK QuantumX MX1615B data acquisition system programmed at a sampling frequency of 1 Hz. Fig. 2a shows a view and a front scheme of the tensile test setup, specifying the main dimensions and the characteristics of the different devices.

Table 1
Mechanical properties of bricks and bed-joint mortar obtained experimentally (coefficients of variation in parentheses).

		at 20 °C	after 200 °C	after 400 °C	after 600 °C
Compressive strength (MPa)	Bricks	13.9 (10.4%)	Not tested	Not tested	13.2 (9.3%)
	Bed-joint mortar	8.4 (8.7%)	9.2 (6.8%)	7.1 (10.0%)	5.7 (4.3%)
Flexural strength (MPa)	Bricks	4.2 (16.9%)	Not tested	Not tested	3.5 (11.9%)
	Bed-joint mortar	1.2 (14.3%)	1.1 (7.6%)	0.7 (16.9%)	0.5 (3.6%)

2.3. Non-destructive tests

To evaluate the degradation of mechanical properties of UHPC after exposure to high temperatures, the evolution of the dynamic modulus of elasticity was studied by means of non-destructive tests. On the one hand, the 160×40×40 mm^3 prismatic samples were subjected to ultrasonic wave propagation tests according to ASTM D2845–08 [58], for which a Proceq Pundit Lab + device was used for data acquisition and processing, equipped with a 250 kHz wave transducers set. The tests were performed along the axial direction of the specimens and an ultrasonic couplant was applied to enhance sound transmission. Once the velocities of the compression (V_p) and shear (V_s) waves were obtained, as well as the density of the mortar (ρ), the dynamic modulus of elasticity can be calculated with Eq. (1).

$$E_{dyn} = \frac{\rho \cdot V_s^2 (3V_p^2 - 4V_s^2)}{V_p^2 - V_s^2} \quad (1)$$

On the other hand, in the UHPC tensile coupons, the fundamental bending resonance frequency was determined according to ASTM E1875–20a [59]. The specimens were tested simply supported on two elastomers at a distance of 0.224 the length of the coupon, from both ends. An Erudite MKIV (PC1004) was used as excitation equipment, acting in the center of the specimen. A PCB 333B50 accelerometer with a sensitivity of 1000 mV/g was attached at one end of the specimen, connected to a HBK QuantumX MX1601B datalogger, for signal recording and processing. The dynamic modulus of elasticity can be computed with Eq. (2), once determined the fundamental bending resonance frequency (f_f), and the mass (m), length (L), width (b) and thickness (t) of the specimen.

$$E_{dyn} = 0.9465 \left(\frac{m \cdot f_f^2}{b} \right) \left(\frac{L^3}{t^3} \right) \left[1 + 6.585 \left(\frac{t}{L} \right)^2 \right] \quad (2)$$

2.4. UHPC-to-masonry bond test

A parameter that is considered very relevant for the objectives of this research is the bond capacity of UHPC on the masonry substrate. To determine this property, a shear test with three bricks and two concrete joints was designed according to EN 1052–3:2002 [60], as shown in Fig. 2b. The tests were carried out on the same press as that used for the tensile coupons, but on this occasion equipped with a 300 kN load cell, and also programmed by displacement control at a constant rate of 0.2 mm/min until failure. A spherical-seat plate was used to apply the load, and a system of plates and round bars was designed for the placement of the specimen, following the recommendations of the

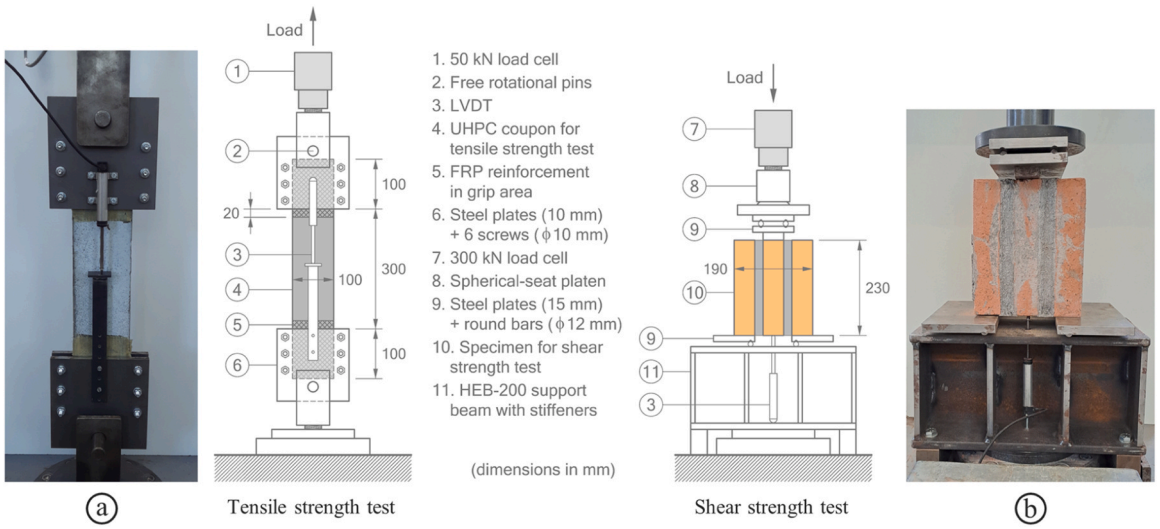

Fig. 2. Detail of test setups: (a) tensile strength test on UHPC coupons; (b) shear strength test to analyze UHPC-to-masonry bond.

European standard. The setup was equipped with two LVTDs to measure the vertical displacement of the central brick, with the same data acquisition system and identical sampling frequency as those described in the previous section.

The bond capacity of UHPC depend to a large extent on the surface preparation, as has recently been reported for the case of concrete [42] or stone [45] substrates. To analyze the bond on masonry, two different types of specimens were designed: samples with flush joints (F) and samples with raked joints (R), in order to simulate two situations frequently found in case of strengthening a wall in a real building. A total of 18 specimens were produced, 9 with flush joints and 9 with raked joints. A water-cooled saw with a diamond blade was used to cut the raked specimens. For the production of the samples, the bricks were placed previously saturated with water inside a removable mold, and the UHPC was immediately poured onto the joints and smoothed out with a smooth-edged metal spatula. The molds were retired after 24 hours and the specimens were covered with polyethylene sheets, which were kept for 28 days under ambient laboratory conditions. The characteristics and dimensions of the two types of specimens manufactured are shown in Fig. 3.

To analyze the effect of high temperatures on the UHPC-to-masonry bond, the specimens were heated to different temperatures in series of three samples. To determine the temperature levels to be reached in this case, the results of the previous tests on prismatic samples and UHPC coupons, described in Section 3.1, were analyzed. From these tests it can be basically concluded: (i) the material retains its properties relatively intact up to 200 °C; (ii) shows a significant loss of its mechanical capacity between 400 and 600 °C; and (iii) it is severely degraded and practically useless at 800 °C. After analyzing these results, it was decided to perform the shear tests at 20 °C, and after exposure to 400 and 600 °C. The heat treatments were carried out in the same oven and with the same heating curves presented in the previous sections. It is important to remark that before performing the shear tests, the series tested at room temperature were dried for 48 hours at 105 °C, in order to homogenize the conditions of the specimens as much as possible, since the series subjected to 400 and 600 °C were completely dry after the heating process.

2.5. Confinement of masonry columns with UHPC

To analyze the strengthening capacity of UHPC by confinement, 10 masonry columns of dimensions 230×230×610 mm^3 were built. Each column was composed of 10 brick courses and 12 mm thick mortar joints (approximately). The brick corners were previously cut at 45° as shown in Fig. 4., in order to avoid an excessive stress concentration at the edges that may cause a premature failure of the UHPC jacket. As mentioned in Section 2.1, a natural hydraulic lime mortar was used for the production of the masonry elements, so the columns were kept for a period of 90 days in ambient laboratory conditions to ensure sufficient curing time.

After curing, 6 of the 10 columns were confined with UHPC in molds with a clear internal dimension of 300×300 mm^2 in order to produce a 35 mm thick jacket, as shown in Fig. 4. To avoid transmitting compressive loads to this UHPC jacket and to evaluate only its

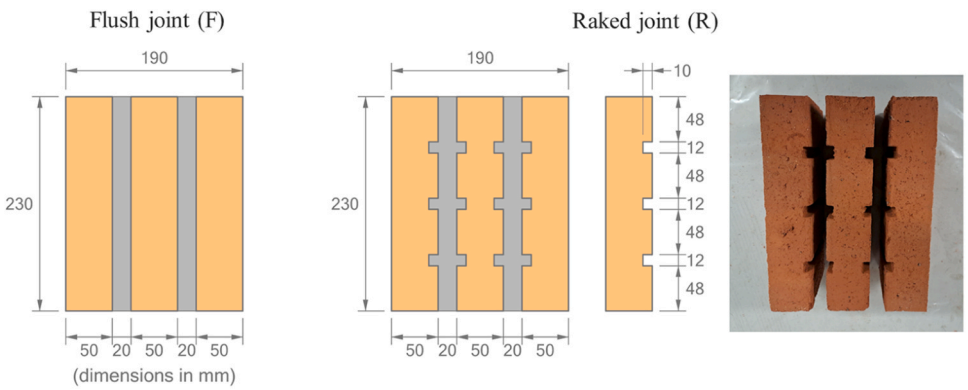

Fig. 3. Detail of specimens prepared for UHPC-to-masonry bond tests.

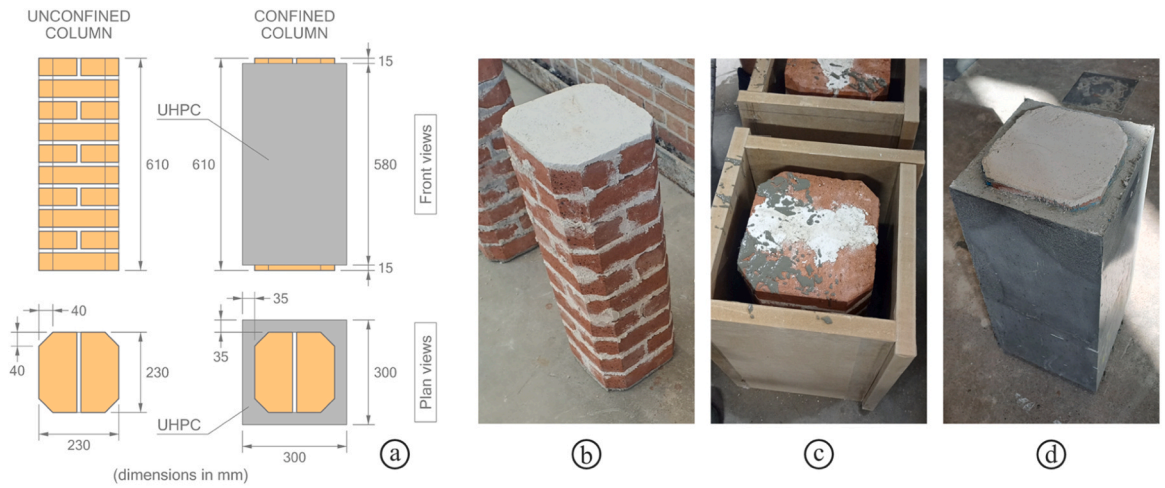

Fig. 4. Column manufacturing: (a) plan and front schemes; (b) unconfined column; (c) detail of mould arrangement; (d) UHPC confined column.

confinement capacity, a gap of approximately 15 mm was left without concrete at both ends of the columns. The strengthening process basically involved the following steps: (i) cleaning of the sides of the columns by means of a steel wire brush and compressed air; (ii) pre-wetting of the masonry substrate to avoid water absorption from UHPC; (iii) mold installation and UHPC pouring; (iv) removal of the mold after 24 hours and protection of specimens with polyethylene sheets; and (v) cured under ambient laboratory conditions for 28 days.

The experimental campaign of the columns was designed as specified in Table 2. On this occasion, specimens were tested at room temperature and after a single exposure level of 600 °C. This temperature was determined on the basis of the results previously obtained in the UHPC tests, as explained in the previous section. The heat treatment was carried out in the same oven described above, programmed with an increasing heating curve of 10 °C/min up to 600 °C, although in this case the target temperature was kept constant for two hours. The specimens then remained in the switched-off oven for an additional 24 hours until reaching the ambient laboratory temperature, as in the other tests described in the previous sections. For temperature monitoring, two thermocouples were installed, one on the outer surface of the UHPC and the other at the UHPC-masonry interface. The data revealed that the thermocouple at the UHPC-masonry interface reached a temperature of approximately 550 °C when disconnecting the oven, although one hour later it showed a maximum peak close to 600 °C. Therefore, the process of heating the specimens was considered sufficiently effective.

The columns were tested in uniaxial compression in a hydraulic press equipped with a 700 kN load cell. To improve contact with the press plates, the ends of the specimens were previously regularized with a layer of mortar. A spherical-seat platen was used to apply the load, in order to correct possible manufacturing or centering errors in the columns. The tests were performed under displacement control at a constant rate of 0.4 mm/min until failure. A set of LVDTs attached with chemical anchors to the sides of the specimens were used to monitor vertical deformations, connected to the same data acquisition equipment and with the same sampling frequency as indicated in the previous sections. Fig. 5 includes two images of the uniaxial compression test for a column from the C20 set (Fig. 5a), and another from the C20U set (Fig. 5b), showing the arrangement of the LVDTs on the specimens.

Table 2
Summary of experimental campaign with masonry columns and panels.

		Temperature	ID	Samples
Columns	Unconfined	At 20 °C	C20-i	i = 1,2
		After 600 °C	C600-i	i = 1,2
	UHPC confined	At 20 °C	C20U-i	i = 1,2,3
		After 600 °C	C600U-i	i = 1,2,3
Panels	Unreinforced	At 20 °C	P20-i	i = 1,2,3
		After 600 °C	P600-i	i = 1,2,3
	UHPC reinforced	At 20 °C	P20U-i	i = 1,2,3
		After 600 °C	P600U-i	i = 1,2,3

2.6. Shear strengthening of masonry panels with UHPC

Finally, to analyze the capacity of UHPC to increase the shear strength of masonry walls under in-plane loads, 12 panels of dimensions 610×610×230 mm^3 were prepared, formed by two brick leaves in stretched bond (Fig. 6a). Each specimen was composed of 10 brick courses and approximately 12 mm thick mortar joints, which were raked out as the panels were built, in order to improve the UHPC-to-substrate bond (Fig. 6b). The specimens were also kept for a 90-day curing period under ambient laboratory conditions, as were the columns. Once this period was completed, six panels were strengthened on both sides with a 20 mm thick layer of UHPC (Fig. 6c). For the application of the reinforcements, the same procedure described above for the case of the columns was basically followed. However, to facilitate the UHPC casting process, the panels were placed in horizontal position and the strengthening was done in two consecutive days, turning the specimens after 24 hours to cast the concrete layer on the opposite side. Obviously, this was a laboratory sample manufacturing process, while in a real building a formwork would be required and the UHPC would be poured from the top. Once the reinforcements were applied, the specimens were kept covered with polyethylene sheets for an additional 28 days.

The design of the experimental campaign for the panels is detailed in Table 2. A single exposure temperature of 600 °C was adopted, as justified in the previous section for the case of the columns, with the same heating process. All the panels were tested in diagonal compression with the same hydraulic actuator as indicated in the previous section, and with identical parameters to those explained for the columns. The specimens were placed between two loading shoes made of 10 mm thick welded steel plates. To improve the contact with the masonry, the bearing surfaces were previously regularized with a layer of mortar. For strain monitoring, each panel was instrumented with two LVDTs oriented along both main diagonals, in order to determine the elongation in the X-direction and the shortening in the Y-direction. The gage length was 400 mm for both LVDTs. The same data acquisition system indicated in the previous sections was used, with the same sampling frequency. Fig. 5c shows an image of the diagonal compression test setup, for a panel corresponding to the P20U set.

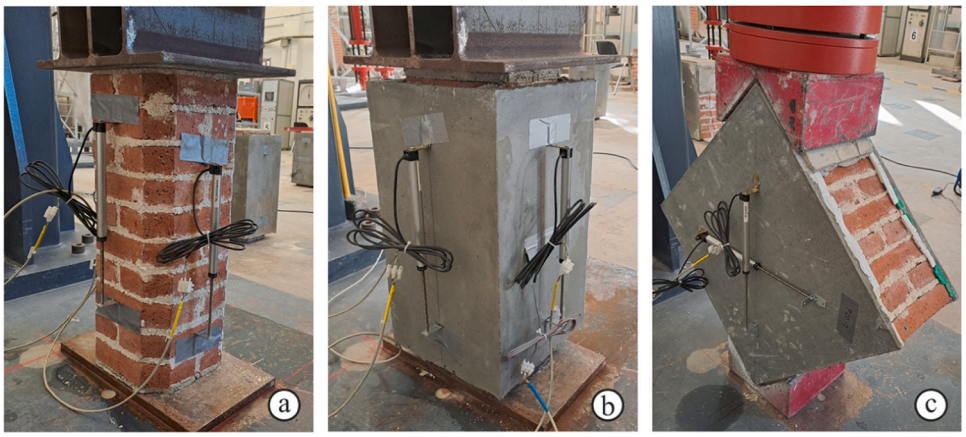

Fig. 5. Test setups: (a) uniaxial compression, unconfined column; (b) uniaxial compression, confined column; (c) diagonal compression, strengthened masonry panel.

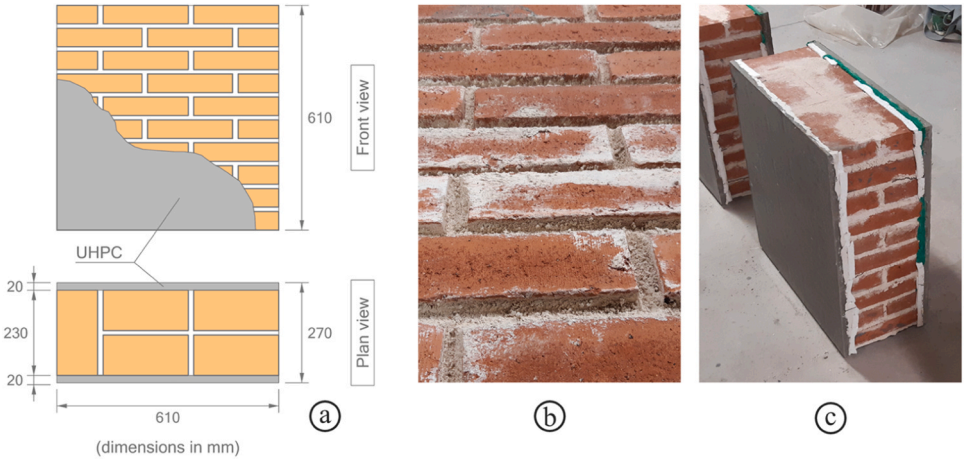

Fig. 6. Panel manufacturing: (a) plan and front scheme; (b) detail of raked joints to improve UHPC-to-substrate bond; (c) masonry panel strengthened with UHPC.

3. Results and discussion

This section presents and discusses the results obtained experimentally. Firstly, the loss of mechanical properties of UHPC after exposure to high temperatures is analyzed, by both destructive and non-destructive tests. Secondly, the UHPC-to-masonry bond capacity is evaluated, as a function of surface preparation and temperature exposure. Finally, the results of compression tests on columns and diagonal compression tests on panels are discussed and compared with the predictions of some design guides, as described in Section 1.

3.1. Mechanical properties of UHPC after exposure to high temperatures

The mechanical properties of UHPC obtained experimentally are summarized in Table 3, for the five temperature levels studied, including the corresponding coefficients of variation in parentheses. This table shows the results of flexural and compression tests on 160×40×40 mm^3 specimens (Section 2.1), tensile tests on 500×100×10 mm^3 coupons (Section 2.2) and non-destructive tests in both cases (Section 2.3). Fig. 7a shows the normalized residual strengths, in order to easily visualize the loss of mechanical properties of the material as a function of temperature. On the other hand, Fig. 7b shows the evolution of the dynamic modulus of elasticity, determined by the two procedures already described, and discussed below. As can be seen, UHPC retains its compressive and flexural strength up to 400 °C, while these properties exhibit a reduction of about 40% after exposure to 600 °C, due to chemical decomposition of cement compounds beyond 500 °C [50]. At 800 °C, the results reveal a strong degradation of the material, with strength drops above 80%.

Table 3
Mechanical properties of UHPC after exposure to high temperatures (coefficients of variation in parentheses).

	at 20 °C	after 200 °C	after 400 °C	after 600 °C	after 800 °C
Compressive strength (MPa)	118.1 (1.9%)	126.6 (1.7%)	122.8 (1.8%)	73.8 (8.9%)	23.8 (1.8%)
Flexural strength (MPa)	27.9 (16.9%)	27.8 (6.1%)	26.1 (1.4%)	17.2 (12.4%)	3.5 (5.2%)
Tensile strength (MPa)	7.5 (7.8%)	7.2 (6.4%)	4.3 (8.7%)	3.4 (13.6%)	0
Modulus of elasticity (MPa)[a]	39206 (1.6%)	37750 (1.4%)	30160 (1.1%)	15406 (3.1%)	6226 (2.4%)
Modulus of elasticity (MPa)[b]	33619 (11.5%)	27004 (10.5%)	19428 (5.0%)	10036 (9.1%)	0

[a] Dynamic modulus from ultrasonic wave propagation tests in 160×40×40 mm^3 mortar samples
[b] Dynamic modulus from sonic resonance tests in 500×100×10 mm^3 tensile coupons

Regarding tensile tests of UHPC coupons, the stress-strain curves obtained experimentally are shown in Fig. 8. To calculate the tensile stress, the applied load is divided by the cross section of the specimen, measured in each sample by means of a micrometer with a precision of

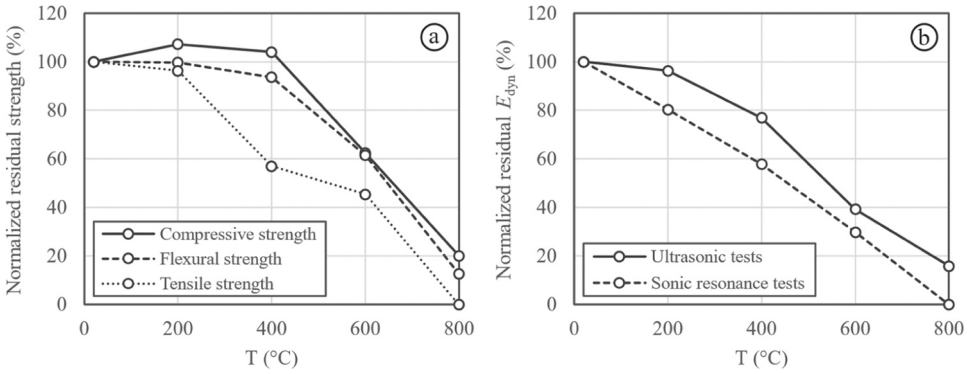

Fig. 7. Evolution of UHPC mechanical properties as a function of temperature: (a) compressive, flexural and tensile strength; (b) dynamic modulus of elasticity. Normalized residual values in all cases.

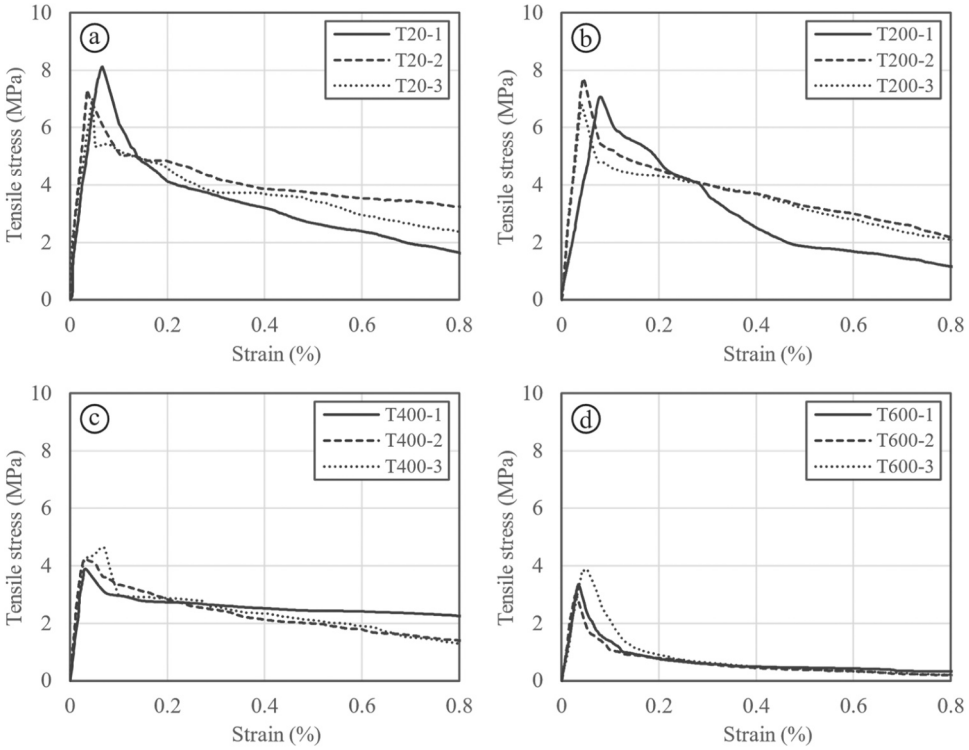

Fig. 8. Tensile stress-strain curves for UHPC coupons: (a) tested at room temperature; (b) after 200 °C; (c) after 400 °C; (d) after 600 °C.

0.01 mm. The strain is determined from the average values of the two LVDTs installed on both sides of the coupon. The curves are only plotted up to 600 °C, as after exposure to 800 °C it was found that the UHPC was completely degraded, and the coupons could be easily cracked by applying a slight tensile load with the hands. In these conditions, the tensile strength is considered to be virtually zero. As the curves show, the tensile behavior of UHPC is characterized by an approximately linear response until the peak tensile stress is reached. The tensile strength included in Table 3 is computed as the average value of this peak stress, for the three samples tested in each set. This point corresponds to the cracking of the specimen, which results in an abrupt decrease in the stress-strain curves. After this point, as can be seen, the slope of the curves becomes smoother as tensile stresses are transferred to the steel fibers. Analyzing Fig. 7a, it can be clearly observed how UHPC retains its tensile strength at moderate temperatures. However, the thermal strain mismatch between the different components (steel fibers, aggregates and cement) leads to microcrack development and fiber anchorage issues [48,50], resulting in a significant loss of strength above 40% after 400 °C and almost 60% after 600 °C, while after 800 °C the material loses all its mechanical capacity, as previously mentioned.

As commented above, Table 3 also includes the results of the dynamic modulus of elasticity obtained by the two techniques explained. Due to the strong degradation shown by the coupons after exposure to 800 °C, it was not possible to perform the sonic resonance test, so it is assumed that the value of E_{dyn} is virtually zero in this set. Analyzing the normalized residual values plotted in Fig. 7b, it can be seen that the dynamic modulus of elasticity shows an approximately linear decrease as the exposure temperature is increased, with the sonic resonance method showing higher reductions and a clearer trend.

To conclude this section, Fig. 9 shows a specimen corresponding to each of the series analyzed after the destructive tests. As can be seen, there are no appreciable visible differences between the specimens tested at room temperature or after exposure to 200 °C, confirming that the material remains relatively intact at moderate temperatures. In the coupons tested in tensile, failure was caused by the appearance of a single crack perpendicular to the direction of the applied load, while the

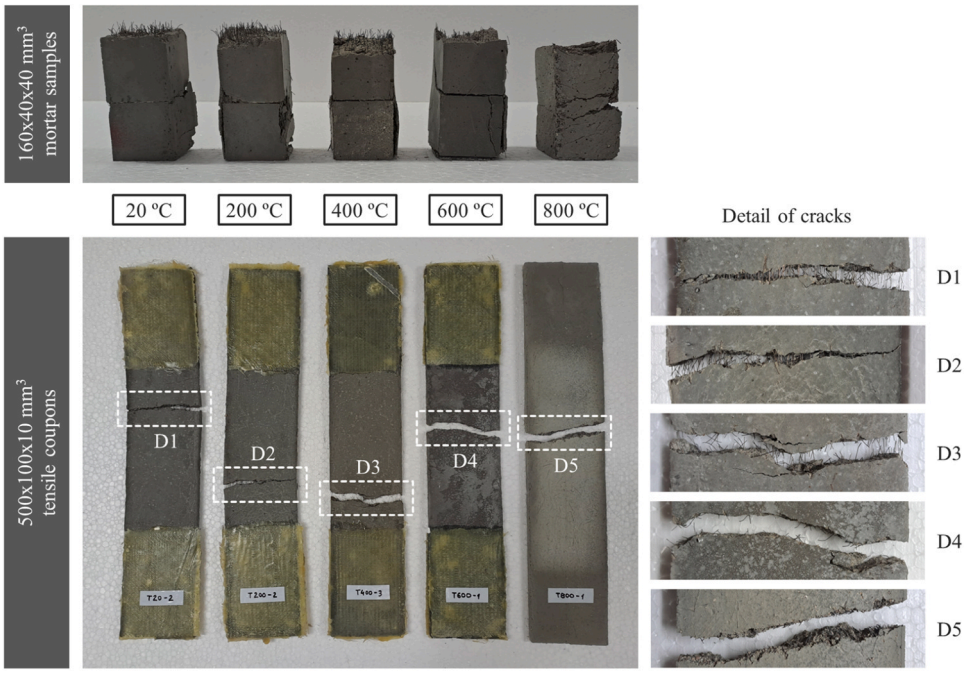

Fig. 9. UHPC specimens after destructive tests: 160×40×40 mm^3 mortar samples and 500×100×10 mm^3 tensile coupons.

steel fibers kept the specimens attached until the end of the test. After exposure to 400 °C, the UHPC was clearly affected by the effect of temperature. The crack in the coupons progressed rapidly after the maximum load was reached, and the specimens were split into two parts. The fracture showed that approximately 50% of the fibers failed under tension, which corresponds to the significant strength decrease that can be observed in Fig. 7a. After exposure to 600 °C, the fibers practically disappeared, as can be seen both in the prismatic samples and in the coupons, and the mechanical capacity of the material was seriously compromised. This behavior is clearly evident in the curves of Fig. 8d, which show how the absence of fibers disables the development of a certain mechanical capacity in the post-peak phase, which can be observed in the rest of the series tested. Finally, after being exposed to 800 °C, the prismatic samples partially preserved their integrity, but the coupons were completely degraded and could easily be broken by hand, as mentioned above. On examining the fractures, no trace of the fibers could be found after exposure to this temperature.

3.2. UHPC-to-masonry bond depending on temperature and substrate preparation

The results of the UHPC-to-masonry bond tests are shown in Fig. 10 as load vs. slip curves, adopting the average values provided by the two LVDTs arranged as described in Section 2.4. On the other hand, Table 4 provides data for the peak load, depending on joint type and exposure temperature. In this table, the shear strength is calculated according to Eq. (3), where A_i is the cross-sectional area of the specimen parallel to the bed joints, i.e., 110×230 mm^2 [60].

Table 4
UHPC-to-masonry bond: experimental results for peak load (coefficients of variation in parentheses).

		at 20 °C	after 400 °C	after 600 °C
Maximum load, V_{max} (kN)	Flush joint (F)	55.48	53.19	32.95
	Raked joint (R)	71.43	57.96	53.00
Shear strength, τ (MPa)	Flush joint (F)	1.10 (1.63%)	1.05 (10.39%)	0.65 (12.53%)
	Raked joint (R)	1.41 (3.06%)	1.15 (6.98%)	1.05 (4.33%)
Maximum slip, s (mm)	Flush joint (F)	0.78 (18.31%)	0.68 (7.08%)	0.60 (22.71%)
	Raked joint (R)	0.76 (3.64%)	0.71 (13.37%)	0.62 (8.66%)

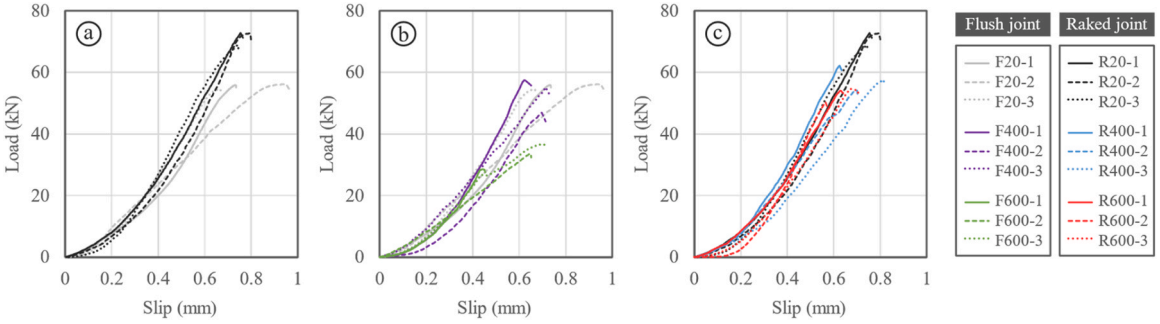

Fig. 10. UHPC-to-masonry bond: (a) flush vs. raked joint at room temperature; (b) flush joint at room temperature and after 400 and 600 °C; (c) raked joint at room temperature and after 400 and 600 °C.

$$\tau = \frac{V_{max}}{2A_i} \quad (3)$$

As can be seen, at room temperature, a 28% increase in shear strength is achieved with the raked joints (Fig. 10a). In a real application in a building with flush joint masonry walls, it could therefore be interesting to prepare the substrate in advance by raking out these joints, in order to improve the efficiency of the UHPC strengthening layers. Analyzing the effect of temperature, it can be seen that in the specimens with flush joints the shear strength is retained up to 400 °C, while after exposure to 600 °C a decrease of about 40% is registered (Fig. 10b). The specimens with raked joints, on the other hand, seem to exhibit a better response under these conditions, with maximum strength drops by 25% after exposure to 600 °C (Fig. 10c). In any case, it should be noted that in all the tested series there were brittle failures and the post-peak phase observed in the tensile tests (Fig. 8) was not found. Consequently, it will be crucial to consider this circumstance in the design phase of the strengthening of a masonry member with UHPC, adopting appropriate safety factors to prevent these failures.

In order to analyze the failure modes obtained, Fig. 11 shows the classification proposed by the European standard EN 1052–3:2002 [60]. In case of poor bonding conditions between UHPC and masonry substrate, failures A and B would be expected, usually in applications on smooth surfaces or with possible manufacturing defects (insufficiently clean substrates, lack of wetting, or inadequate curing conditions, for example). Failure C may occur in case of weak mortars applied on substrates with higher mechanical capacity. Failure D would correspond to high strength mortars applied on weaker substrates. This failure mode is the one that a priori should be obtained in this investigation, at least at room temperature scenario, taking into account the properties of the materials used (Section 2.1). Finally, with respect to failure E, it may occur in case of mortars and substrates with similar mechanical properties and optimal bonding conditions.

A representative sample of each of the series tested is shown in Fig. 12. Analyzing first the behavior of the specimens with flush joints, it is observed that the failure was caused by the fracture of the brick (failure D), leaving a layer of clay approximately 5–10 mm thick remained closely attached to the UHPC. Both materials were found to bond strongly to each other and there were no significant differences between the samples tested at room temperature and those subjected to 400 °C. However, the behavior changed drastically after exposure to 600 °C, with debonding at the UHPC-brick interface on one (failure A) or both sides (failure B). This failure mode is clearly reflected in the shear strength decrease registered in this series (Fig. 10b). It can be concluded, therefore, that exposure to high temperatures can significantly reduce the UHPC-to-masonry bond in case of walls with flush joints.

Regarding specimens with raked joints, the bricks were seen to break in all cases (failure D) regardless of whatever temperature they had been subjected to. The plane of the fracture coincided approximately with the bottom of the raked joint and a slight debonding at the UHPC-brick interface was only found in some of the specimens exposed to 600 °C which, however, did not result in a significant strength drop (Fig. 10c). Consequently, it can be concluded that the effect of raking out the joints can be highly beneficial from the point of view of fire resistance of these reinforcements and could prevent premature debonding of the UHPC layers from the masonry substrates. In any case, in future research it will be interesting to analyze the possible addition of mechanical connectors as an alternative solution to the raked joints, as this solution could considerably reduce the costs and execution times of applications in real buildings.

3.3. Analysis of column confinement and comparison with design guides

For the discussion of the results of the columns tested in compression, the failure modes obtained in the different series studied are presented first. In the unconfined columns (Fig. 13a) it can be seen that the typical vertical cracks of masonry elements under compression appeared in the final phases of the tests, with relatively fragile failures. All the samples tested at whatever temperature showed the same behavior. In the confined columns, the failure started from a vertical crack in the center of each side (Fig. 13b), spreading to the full height of the UHPC jacket. These cracks appeared at around the time that the maximum load was applied, and then gradually widened during the rest of the test. In all cases, it was observed in the later stages that the crack on one side spread much faster than the others, until the specimen failed (Fig. 13c). Overall, in the post-peak phase, it was found that UHPC jacket provided the column with ductility, since the actuator either kept a relatively constant load or registered a slight drop that was prolonged in time, with the response being largely dependent on the temperature it had been exposed to. In the specimens tested at room temperature, the steel fibers were seen to effectively bridge the cracks (Fig. 13d), which resulted in a greater capacity to keep the load practically constant, with slight decreases in the final stages of the tests. However, in the columns exposed to 600 °C, the tensile capacity of the fibers was severely affected (Fig. 13e), which resulted in a much more pronounced load drop. As can be seen, there is a direct correspondence between the cracking of the jacket as a function of temperature and the results obtained in the tensile tests on UHPC coupons, as described in Section 3.1 (Fig. 8a, d and Fig. 9). It is also important to highlight the fact that the cracks affected the LVDTs anchorage in most cases, as can be clearly seen in Fig. 13b. For this reason, no reliable data are available to calculate the axial deformation of the columns and, consequently, the corresponding stress-strain curves cannot be provided. The analysis below is therefore given in terms of maximum compressive strength, since the post-peak behavior could not be properly characterized. It is suggested to consider this circumstance in future research and to design other monitoring strategies that can solve this problem, such as analysis by contactless techniques, e.g. Digital Image Correlation (DIC), or systems based on Distributed Fiber Optic Sensors (DFOS), which have been effectively tested in previous studies on masonry elements [61,62].

The results obtained are shown in Table 5 for all the specimens tested, in terms of maximum compressive load (F_{max}) and corresponding compressive strength, for both unconfined (f_{mo}) or confined (f_{mc}) columns, including average values and coefficients of variation in

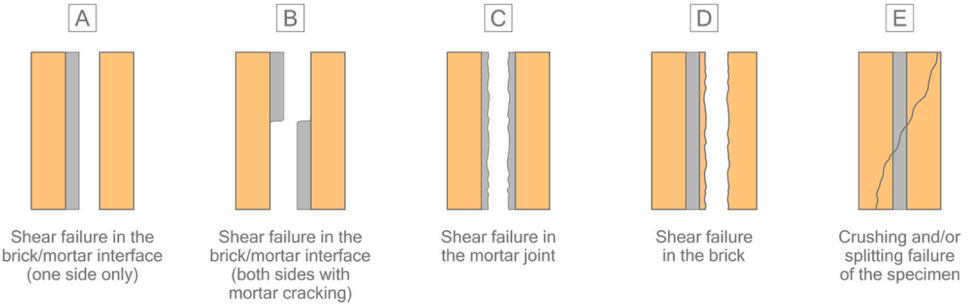

Fig. 11. UHPC-to-masonry bond: failure modes according to EN 1052-3:2002 [60].

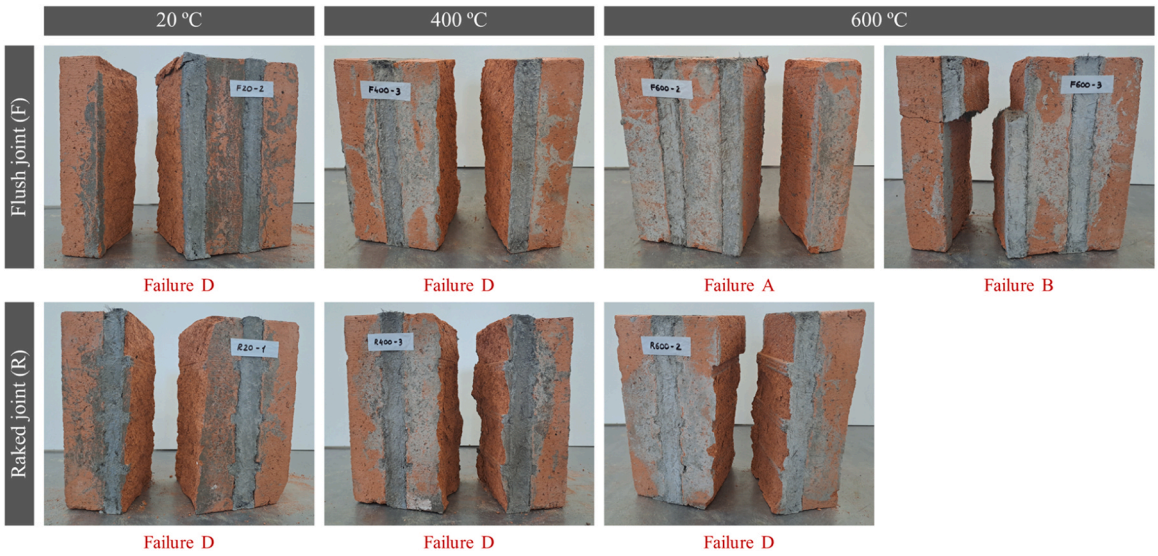

Fig. 12. UHPC-to-masonry bond: examples of failure modes obtained as a function of temperature and substrate preparation.

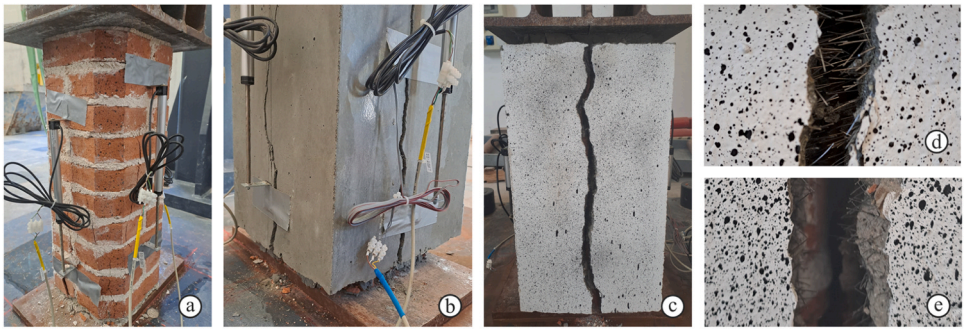

Fig. 13. Uniaxial compression tests in columns: (a) unconfined column; (b) crack patterns in confined column; (c) confined column at the end of the test; (d) crack detail in confined column at room temperature; (e) crack detail in confined column after exposure to 600 °C.

Table 5
Compressive strength for unconfined (f_{mo}) or confined (f_{mc}) columns: experimental results and design guides prediction (coefficients of variation in parentheses).

ID	F_{max} (kN)	f_{mo} (MPa)	Average f_{mo} (MPa)	f_{mc} (MPa)	Average f_{mc} (MPa)	Prediction f_{mc} (MPa)	
						ACI	CNR
C20-1	267.0	5.37	5.15	-	-	-	-
C20-2	245.0	4.93	(6.07%)	-			
C600-1	148.6	2.99	2.70	-	-	-	-
C600-2	119.8	2.41	(15.18%)	-			
C20U-1	418.2	-	-	8.41	9.68	8.86	9.12
C20U-2	508.3	-		10.23	(11.32%)		
C20U-3	516.3	-		10.39			
C600U-1	482.0	-	-	9.70	9.05 (10.27%)	6.84	7.56
C600U-2	396.8	-		7.98			
C600U-3	470.2	-		9.46			

parentheses. For the calculation of the compressive strength, the masonry cross-section is adopted in both cases (without considering the thickness of the UHPC) because, as specified in Section 2.5, a gap of approximately 15 mm was kept at the ends of the columns to avoid direct vertical compression on the jacket. Analyzing the response of the unconfined columns, it can be seen that the effect of high temperature reduces the compressive strength by approximately 50%. In these specimens, a significant degradation was observed after exposure to 600 °C, with loss of masonry assembly and bond defects between the bricks and the bed-joint mortar in some areas. Similar degradation was also observed in previous studies with masonry walls subjected to real fire [31]. Regarding confined columns, it can be seen that UHPC jacket approximately doubled the compressive strength, with respect to C20 set. Contrary to what might be expected a priori, the experimental results show that the compressive strength of confined columns is practically identical, both for the specimens tested at room temperature and those exposed to 600 °C. Undoubtedly, in addition to confinement, the UHPC layer seems to produce an insulating effect on the masonry core. In view of the results, it can be concluded that the strengthening of masonry columns with UHPC jackets can be a very effective solution, even under high temperature exposure or fire scenarios.

To complete the analysis of the behavior of confined columns, it is considered interesting to compare the results obtained experimentally with the predictions of some design guides. As there are no published standards available at the present time for strengthening masonry structures with UHPC, this study adopts the column confinement models proposed by the main guides for TRM, specifically the American ACI 549.6R-20 [52] and the Italian CNR-DT 215/2018 [53]. One of the main novelties of this work is precisely to check whether these models, despite not having been specifically formulated for confinement with UHPC or after exposure to high temperatures, could be satisfactorily used under the hypotheses proposed in this research. It should be mentioned that the notation defined in both guides has been slightly modified, in order

to homogenize the formulation between the two documents.

The maximum confined masonry compressive strength (f_{mc}) can be obtained from unconfined strength (f_{mo}) by Eq. (4) and Eq. (5), as specified in the American and Italian guides, respectively.

$$\text{ACI}: f_{mc} = f_{mo} + 3.3 \cdot \Psi_f \cdot f_{l,eff} \tag{4}$$

$$\text{CNR}: f_{mc} = f_{mo}\left[1 + k' \left(\frac{f_{l,eff}}{f_{mo}}\right)^{\alpha_1}\right] \tag{5}$$

In these expressions: $\Psi_f = 0.95$ is a reduction factor, which is not considered in this study (the formulation has been found to better match the experimental results without this factor); $f_{l,eff}$ is the effective confining pressure; k' is a coefficient of strength increase, that can be obtained by Eq. (6); and the exponent α_1 can be assumed equal to 0.5, in absence of further experimental evidence.

$$k' = \alpha_2 \left(\frac{g_m}{1000}\right)^{\alpha_3} \tag{6}$$

In this equation: g_m is the masonry mass density, expressed in kg/m^3; and the coefficients α_2 and α_3 should be assumed prudently equal to 1 if experimental results are no available to justify higher values. To determine the masonry density, the columns were measured and weighed, obtaining an average value of 1648 kg/m^3 (C20 set) and 1483 kg/m^3 (C600 set), so $k' \approx 1.65$ for the columns tested at room temperature and $k' \approx 1.48$ for the specimens exposed to 600 °C.

Regarding the effective confining pressure, it can be calculated by Eq. (7), as a function of the maximum confinement pressure (f_l), the coefficient of horizontal efficiency or shape factor (k_h) and the coefficient of vertical efficiency (k_v).

$$f_{l,eff} = k_h \cdot k_v \cdot f_l \tag{7}$$

The maximum confinement pressure (f_l) is defined in both guides for the case of TRM jackets according to Eq. (8), where: n_f is the number of layers of fabric reinforcement; t_f is the equivalent thickness of the fibers in the direction orthogonal to the axis of the column; E_f is the elastic modulus of the reinforcement, which ACI assumes to be the modulus of the cracked phase determined in tensile TRM coupons tests, while CNR directly adopts the elastic modulus of the dry textile; ε_{fd} represents the design ultimate strain, which each of the guides considers in a different way: ACI sets a limit value of 0.012 for confinement applications, while CNR introduces a conventional limit deformation ($\varepsilon_{lim,conv}$) that takes into account the different failure modes of TRM; and D is the diagonal length of the square cross-section, as specified in Fig. 14.

$$f_l = \frac{2 \cdot n_f \cdot t_f \cdot E_f \cdot \varepsilon_{fd}}{D} \tag{8}$$

To adapt this formulation to the case of UHPC confinement, the following assumptions are made: (i) $n_f \cdot t_f$ is equivalent to the UHPC jacket thickness (t_c, as specified in Fig. 14); and (ii) $E_f \cdot \varepsilon_{fd}$ is equivalent to the UHPC tensile strength (f_t), depending on exposure temperature (Table 3). Consequently, the maximum confinement pressure for the columns strengthened with UHPC jackets is estimated with Eq. (9).

$$f_l = \frac{2 \cdot t_c \cdot f_t}{D} \tag{9}$$

Regarding the coefficient of horizontal efficiency, in case of square section columns, it can be calculated by Eq. (10), where A_m is the masonry cross-section and A_e represents the area of the effectively confined column, provided by Eq. (11). All variables included in these equations are defined in Fig. 14, which also shows one of the strengthened columns exposed to 600 °C, after the compression test.

$$k_h = \frac{A_m}{A_e} \tag{10}$$

$$A_e = A_m - \frac{2(b-2r)^2}{3} \tag{11}$$

Finally, the coefficient of vertical efficiency is only applicable in case of discontinuous wrappings, so $k_v = 1$ is adopted in this study.

The results provided by Eqs. (4) and (5) are included in Table 5. It is important to note that in these equations, the average $f_{mo} = 5.15$ MPa (corresponding to the C20 set) is used both in the columns tested at room temperature and in those exposed to 600 °C. The reason for adopting this value in both cases is that, after the compression tests, it was found that the masonry core was sound and did not show the degradation observed in the C600 set, undoubtedly due to the protection of the UHPC jacket (Fig. 14). It is not reasonable, therefore, to adopt a value $f_{mo} = 2.70$ MPa for the strengthened specimens exposed to 600 °C, since this approach does not faithfully represent reality. The comparison of the experimental results with the theoretical values provided by both confinement models is represented in Fig. 15. As can be seen, in case of the columns tested at room temperature, both guides provide a great level of accuracy, with differences of less than 10%. It can therefore be concluded that the formulation included in these standards, with the adaptations proposed

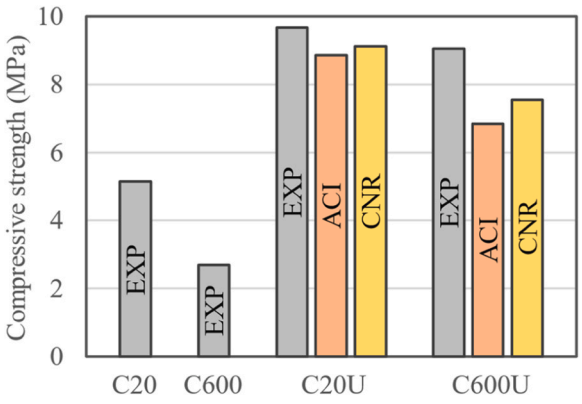

Fig. 15. Column compressive strength: experimental results (EXP) and prediction according to ACI 549.6R-20 [52] and CNR-DT 215/2018 [53].

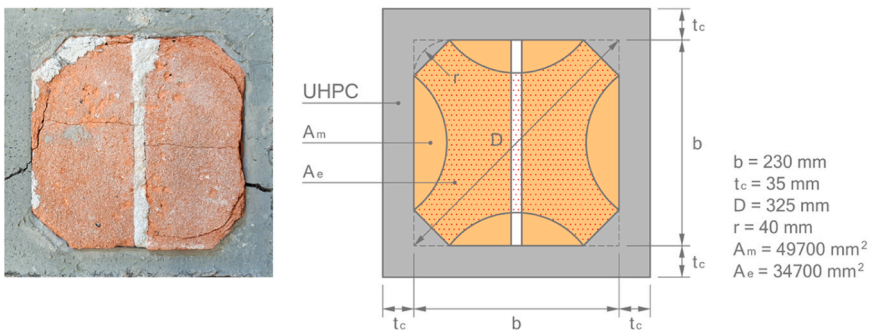

Fig. 14. Example of a strengthened column exposed to 600 °C after the compression test, and confinement scheme with UHPC jacket.

in this study, could be successfully used in case of confinement of masonry columns with UHPC. Of course, this conclusion is limited exclusively to the results obtained in this research, based on a small number of specimens, and should be further validated by more experiments in the future. Regarding the columns exposed to 600 °C, however, it is evident that the theoretical models tend to underestimate the results. The main reason is that the tensile strength of UHPC in Eq. (9) is derived from tensile tests on 10 mm thick coupons exposed to 600 °C on both sides, while the UHPC jacket, thicker and exposed only on one side, seems to exhibit a better response under high temperatures.

3.4. Analysis of shear strengthening of panels and comparison with design guides

In the same way as in the case of columns, and as explained in Section 3.3, to discuss the results of diagonal compression tests on masonry panels, it is convenient to previously present the failure modes obtained. The unreinforced panels tested at room temperature (Fig. 16a) showed brittle failures, with cracking of the specimens along the direction of the main compressed diagonal in a stair-stepped pattern, i.e., cracks following the joints between the bricks and the mortar. The failure mode was similar in the unreinforced panels exposed to 600 °C (Fig. 16b), although in this case the masonry showed greater degradation after cracking and ended in a total collapse. This degradation was mainly attributed to the bonding loss at the brick-mortar interface after exposure to high temperatures, as discussed in previous sections. Regarding the UHPC-reinforced panels, the failure mode was identical, both for the specimens tested at room temperature (Fig. 16c) and those subjected to 600 °C (Fig. 16d). The failure started from a crack observed in the midplane of the panel, but with a noticeable difference: while in the P20U set this crack appeared approximately when the peak load was reached, in the P600U set the cracking was identified from the early stages of the test, and the maximum load supported by the panels was considerably lower. The post-peak phase was characterized in all cases by a slow load decrease as the crack width progressed and the gap between both brick leaves increased. It was found, therefore, that the UHPC reinforcement provided a remarkable ductility to the panels and prevented the brittle failures obtained in the unreinforced specimens. As can be clearly observed, the UHPC layers remained intact in all cases, without any cracks and evidencing a perfect bond with the masonry substrate, even after high temperature exposure, which proved the effectiveness of the surface preparation by raking out the joints (Fig. 6b). On the other hand, it is important to emphasize that the analysis presented below will be carried out only in terms of shear strength because, given the failure modes obtained, it was not possible to properly characterize the post-peak behavior of the strengthened panels. To provide shear stress-strain curves it is necessary to measure the shortening of the diagonal in the load direction (vertical) and the extension of the orthogonal diagonal (horizontal). However, as the crack between both brick leaves progressed, the horizontal LVDT did not record elongations in the post-peak phase, but shortened as the panel deformed. For this reason, no reliable data are available to build the corresponding shear stress-strain curves. In this sense, the use of transverse connectors to avoid the separation between the brick leaves, as suggested by the ACI 549.6R-20 [52] guidelines, could be very appropriate for future investigations.

The experimental results of the diagonal compression tests are shown in Table 6, in which F_{max} is the maximum load reached by each specimen. In addition, the average values of these loads are provided, in terms of in-plane shear capacity of unreinforced (V_{urm}) or reinforced (V_{rm}) masonry panels, including the corresponding coefficients of variation in parentheses. Analyzing first the response of the unreinforced panels, it can be seen that exposure to 600 °C reduced the shear strength by almost 50%, for the reasons already mentioned above. Regarding the strengthened specimens tested at room temperature, it was found that the UHPC layers increased the shear strength by almost 65% (with respect to the P20 set), and provided significant ductility to the panels. In the strengthened specimens tested after 600 °C, it was observed that exposure to high temperatures significantly reduced the effectiveness of the UHPC layers. However, even under these conditions, it was possible to restore the shear capacity of the panels to that of the P20 set, and provide a ductility that they initially lacked. In view of the results, it can

Table 6
In-plane shear capacity of masonry panels: experimental results and design guides prediction (coefficients of variation in parentheses).

ID	F_{max} (kN)	Average V_{urm} (kN)	Average V_{rm} (kN)	ACI prediction		CNR prediction	
				V_f (kN)	V_{rm} (kN)	V_f (kN)	V_{rm} (kN)
P20-1	238.1	204.9 (15.9%)	-	-	-	-	-
P20-2	172.8						
P20-3	203.9						
P600-1	101.4	116.1 (17.9%)	-	-	-	-	-
P600-2	38.3[a]						
P600-3	130.8						
P20U-1	388.0	-	336.6 (13.6%)	182.5	387.4	146.0	350.9
P20U-2	299.8						
P20U-3	322.0						
P600U-1	197.6	-	215.0 (8.8%)	83.0	199.1	66.4	182.5
P600U-2	235.2						
P600U-3	212.0						

[a] The specimen P600-2 is not considered in the average

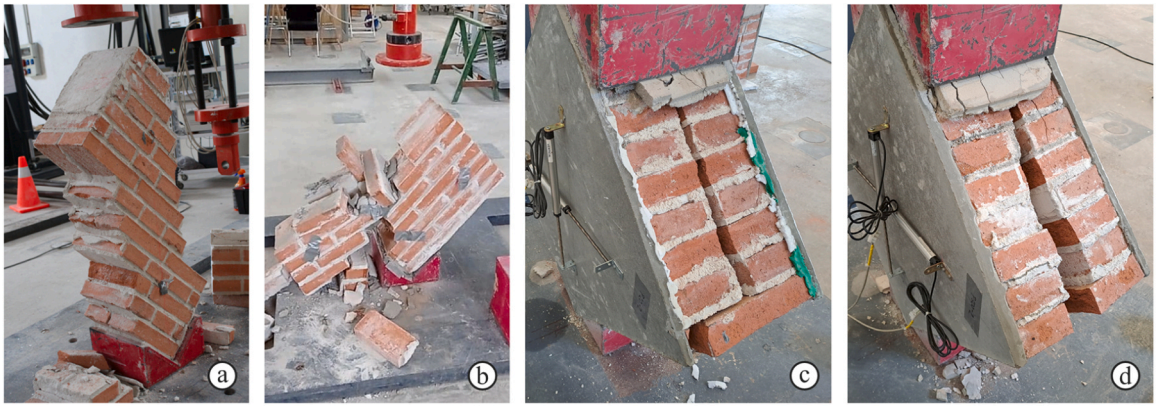

Fig. 16. Diagonal compression tests: (a) unreinforced panel at 20 °C; (b) unreinforced panel after exposure to 600 °C; (c) UHPC reinforced panel at 20 °C; (d) UHPC reinforced panel after exposure to 600 °C.

be concluded that UHPC can offer a potential strengthening solution for masonry walls against in-plane loads, even under high temperatures or fire scenarios, always after a proper surface preparation to guarantee an optimal bond to the masonry substrate. Nevertheless, it will be interesting to explore in future research the possibility of including transverse connectors in case of multi-wythe walls, to prevent the wythe separation [52].

To conclude this section, the experimental results are compared with the predictions of the ACI 549.6R-20 [52] and CNR-DT 215/2018 [53] theoretical models. As in the case of the columns, the aim of this study is to check whether the models developed for in-plane shear capacity of TRM-strengthened masonry walls could be successfully used in case of reinforcement with UHPC layers, both for undamaged walls and after exposure to high temperatures. As in Section 3.3, the notation defined in the guides has been slightly modified to homogenize the formulation between both documents.

The in-plane shear capacity of a strengthened masonry wall (V_{rm}) can be estimated by simply adding the contribution of the reinforcement (V_f) to the shear strength of the unreinforced wall (V_{urm}), as specified in Eq. (12).

$$V_{rm} = V_{urm} + V_f \tag{12}$$

The shear strength of the unreinforced wall can be calculated according to the design standards for masonry structures (e.g. [63]), or it can also be determined experimentally, as in the case of this work. Regarding the contribution of the reinforcement, Eq. (13) and Eq. (14) present the formulation provided by the American and the Italian guides, respectively.

$$\text{ACI}: \; V_f = n_f \cdot t_f \cdot l_f \cdot E_f \cdot \varepsilon_{fd} \tag{13}$$

$$\text{CNR}: \; V_f = \frac{1}{\gamma_{Rd}} n_f \cdot t_f \cdot l_f \cdot \alpha_t \cdot E_f \cdot \varepsilon_{fd} \tag{14}$$

In these equations: n_f, t_f, E_f and ε_{fd} have been previously introduced in Section 3.3; l_f is the dimension of the reinforcement measured orthogonally to the shear force, i.e., the lateral dimension of the panel (610 mm); γ_{Rd} is a partial safety factor equal to 2, which is not considered in this study for a proper comparison between predictions and experimental results; and α_t is a coefficient that, in absence of further experimental evidence, can be assumed equal to 0.8. To adapt the formulation to the case of UHPC-strengthened masonry walls, the same considerations explained in the previous section are assumed, resulting in Eqs. (15) and (16), where: t_c is the total thickness provided by the two UHPC layers (i.e., 40 mm, as specified in Fig. 6a); and f_t is the UHPC tensile strength, depending on exposure temperature (Table 3). As can be seen, the shear strength provided by the Italian guide is 20% lower, due to the application of the coefficient α_t.

$$\text{ACI}: \; V_f = t_c \cdot l_f \cdot f_t \tag{15}$$

$$\text{CNR}: \; V_f = 0.8 \cdot t_c \cdot l_f \cdot f_t \tag{16}$$

The results obtained using both equations are included in Table 6. It should be noted that in the calculation of V_{rm}, a different value of the shear strength of the unreinforced walls is adopted on this occasion: V_{urm} = 204.9 MPa (for the P20U set) and V_{urm} = 116.1 MPa (for the P600U set). It has been decided to adopt these values because, as mentioned above, the masonry core of the UHPC-reinforced panels exposed to 600 °C revealed a certain damage, contrary to what was observed in the case of the columns. This damage was probably due to a larger exposed area of the masonry core (the full thickness of the panel around its entire perimeter). To facilitate the interpretation of the results, Fig. 17 shows the in-plane shear strength of all the series analyzed. This graph is plotted in terms of shear stress (τ), determined according to Eq. (17) from ASTM E519/E519M-21 [64].

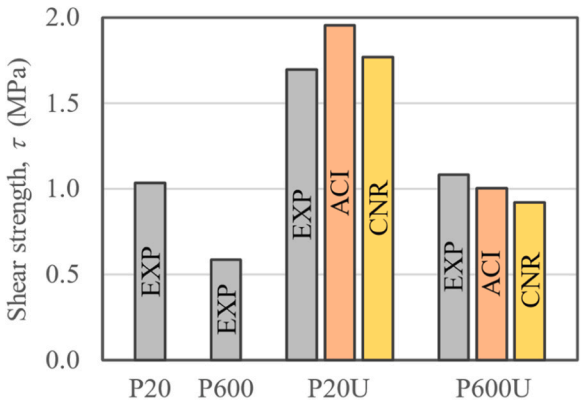

Fig. 17. In-plane shear strength in panels: experimental results (EXP) and prediction according to ACI 549.6R-20 [52] and CNR-DT 215/2018 [53].

$$\tau = \frac{0.707V}{A_n} \tag{17}$$

In this equation: V is the applied load (i.e., V_{urm} or V_{rm}, in each case), and A_n is the net area of the specimen, provided by Eq. (18), where w and h are the width and height of the specimen (610 mm in both cases), t is the thickness of the panel (230 mm), and n is the percent of the gross area of the unit that is solid (1 in this case).

$$A_n = \left(\frac{w+h}{2}\right) \cdot t \cdot n \tag{18}$$

As can be seen, the theoretical models proposed by both guides, with the adaptations suggested in this study, provide a good prediction of the experimental results. In case of the reinforced panels tested at room temperature, it is shown that the model of the Italian guide provides better results, due to the coefficient α_t (which is not included in the ACI model). Regarding the panels exposed to 600 °C, the approximation obtained with both formulations is excellent. It can be concluded, therefore, that these guides could be successfully applied in case of UHPC-strengthened walls, even under high temperatures or fire scenarios. Nevertheless, as in the case of the confined columns, it is necessary to emphasize again the idea that these results have been obtained from a small number of specimens, and should be further validated in future research.

4. Conclusions

This paper presents the results of an experimental study that analyzes the evolution of the mechanical properties of ultra high performance concrete (UHPC) at temperatures up to 800 °C, and its application for the strengthening of masonry members under compressive and in-plane shear loads. The main findings and conclusions to be drawn from this work are summarized as follows:

- The UHPC used in this study retained its mechanical properties relatively intact at moderate temperatures. From the point of view of the objectives of this research, it is crucial the characterization of the tensile strength of the material, which suffered a reduction of over 40% after exposure to 400 °C, and almost 60% after 600 °C. At this temperature, the steel fibers practically disappeared and the mechanical capacity of the UHPC was seriously compromised. After exposure to 800 °C the material was strongly degraded, and the specimens could be easily cracked by applying a slight tensile load with the hands.
- To analyze the UHPC-to-masonry bond, two types of samples were prepared with flush or raked joints, and were tested under shear loads up to 600 °C. At room temperature, the results showed that

raked joints could increase the shear strength by almost 30%. After exposure to 600 °C, debonding occurred at the UHPC-masonry interface in specimens with flush joints and a significant strength decrease was found, while raked joints could prevent this failure mode and provide a better response under these conditions. It can be concluded, therefore, that substrate preparation by raking out the joints is highly recommended for strengthening masonry walls with UHPC, both in normal service conditions and under possible fire scenarios.

- The compressive strength of masonry columns confined with UHPC, tested at room temperature and after exposure to 600 °C, was analyzed. The effect of high temperature was found to cause a reduction in compressive strength of about 50% in the unreinforced columns. Regarding the confined columns, it was observed that UHPC jackets approximately doubled the compressive strength and provided ductility in the post-peak phase. Contrary to what might be expected a priori, the response of confined columns was practically identical, both for the specimens tested at room temperature and those exposed to 600 °C. Consequently, it can be concluded that the strengthening of masonry columns with UHPC jackets can be a very effective solution, even under high temperatures.
- The in-plane shear capacity of masonry panels strengthened with UHPC layers applied on both sides was also evaluated, both at room temperature and after 600 °C. The effect of temperature on the unreinforced panels produced a strength decrease similar to that observed in the columns, over 50%. Regarding the strengthened specimens tested at room temperature, the UHPC layers increased the shear strength by almost 65%, providing high ductility and preventing the brittle failures found in case of unreinforced panels. However, in contrast to the columns, a clear loss of efficiency of the UHPC was detected after exposure to 600 °C. It should be noted that the failure mode of the strengthened panels was by cracking along the midplane of the masonry core in all cases, with separation of both brick leaves. In this sense, it will be interesting to explore in future research the possibility of including transverse connectors to prevent this effect, in case of multi-wythe walls.
- Finally, the experimental results are compared with the predictions of the theoretical models proposed by the American ACI 549.6R-20 and the Italian CNR-DT 215/2018 guidelines, defined for TRM. In case of the confined columns tested at room temperature, both guides provide good accuracy, with differences of less than 10%. Regarding the columns exposed to 600 °C, however, the theoretical models tend to slightly underestimate the results. In case of the UHPC-reinforced panels, the predictions provided by both guides are excellent, both for the specimens tested at room temperature and after 600 °C. In general, it can be concluded that the theoretical models proposed by these guides, with the adaptations suggested in this study, could be successfully used in case of UHPC-strengthened masonry members, even under high temperatures or fire scenarios. In any case, these results are based on a small number of specimens and should be further validated in future research.

CRediT authorship contribution statement

L. Estevan: Writing – original draft, Methodology, Investigation, Conceptualization. **B. Torres:** Writing – review & editing, Methodology, Investigation. **F.J. Baeza:** Writing – review & editing, Methodology, Funding acquisition, Conceptualization. **V. Gattulli:** Writing – review & editing, Conceptualization. **S. Ivorra:** Writing – review & editing, Resources, Funding acquisition.

Declaration of Competing Interest

The authors declare that they have no known competing financial interests or personal relationships that could have appeared to influence the work reported in this paper.

Data availability

Data will be made available on request.

Acknowledgements

The authors would like to acknowledge Mapei Spain and Grupo Puma for the materials supplied in this work. This research has been funded by the Spanish Ministry of Science, Innovation and Universities, grant number RTI2018-101148-B-I00. F. J. Baeza also wants to thank the Spanish Ministry of Education, Culture and Sport for the financial support during his project with Prof. Gattulli in the Programme José Castillejo, grant number CAS15/00223.

References

[1] A.M. Ceci, A. Contento, L. Fanale, D. Galeota, V. Gattulli, M. Lepidi, F. Potenza, Structural performance of the historic and modern buildings of the University of L'Aquila during the seismic events of April 2009, Eng. Struct. 32 (2010) 1899–1924, https://doi.org/10.1016/j.engstruct.2009.12.023.
[2] A. Penna, P. Morandi, M. Rota, C.F. Manzini, F. da Porto, G. Magenes, Performance of masonry buildings during the Emilia 2012 earthquake, Bull. Earthq. Eng. 12 (2014) 2255–2273, https://doi.org/10.1007/s10518-013-9496-6.
[3] J. Toti, V. Gattulli, E. Sacco, Nonlocal damage propagation in the dynamics of masonry elements, Comput. Struct. 152 (2015) 215–227, https://doi.org/10.1016/j.compstruc.2015.01.011.
[4] L. Sorrentino, S. Cattari, F. da Porto, G. Magenes, A. Penna, Seismic behaviour of ordinary masonry buildings during the 2016 central Italy earthquakes, Bull. Earthq. Eng. 17 (2019) 5583–5607, https://doi.org/10.1007/s10518-018-0370-4.
[5] S. Russo, F. Sciarretta, Masonry exposed to high temperatures: mechanical behaviour and properties - An overview, Fire Saf. J. 55 (2013) 69–86, https://doi.org/10.1016/j.firesaf.2012.10.001.
[6] A. Daware, M.Z. Naser, Fire performance of masonry under various testing methods, Constr. Build. Mater. 289 (2021) 123183, https://doi.org/10.1016/j.conbuildmat.2021.123183.
[7] L.A.S. Kouris, T.C. Triantafillou, State-of-the-art on strengthening of masonry structures with textile reinforced mortar (TRM), Constr. Build. Mater. 188 (2018) 1221–1233, https://doi.org/10.1016/j.conbuildmat.2018.08.039.
[8] M. Del Zoppo, M. Di Ludovico, A. Balsamo, A. Prota, Experimental in-plane shear capacity of clay brick masonry panels strengthened with FRCM and FRM composites, J. Compos. Constr. 23 (2019) 04019038, https://doi.org/10.1061/(asce)cc.1943-5614.0000965.
[9] L. Garcia-Ramonda, L. Pelá, P. Roca, G. Camata, In-plane shear behaviour by diagonal compression testing of brick masonry walls strengthened with basalt and steel textile reinforced mortars, Constr. Build. Mater. 240 (2020) 117905, https://doi.org/10.1016/j.conbuildmat.2019.117905.
[10] F. Ferretti, C. Mazzotti, FRCM/SRG strengthened masonry in diagonal compression: experimental results and analytical approach proposal, Constr. Build. Mater. 283 (2021) 122766, https://doi.org/10.1016/j.conbuildmat.2021.122766.
[11] J. Donnini, G. Maracchini, S. Lenci, V. Corinaldesi, E. Quagliarini, TRM reinforced tuff and fired clay brick masonry: experimental and analytical investigation on their in-plane and out-of-plane behavior, Constr. Build. Mater. 272 (2021) 121643, https://doi.org/10.1016/j.conbuildmat.2020.121643.
[12] L. Mercedes, E. Bernat-Maso, L. Gil, In-plane cyclic loading of masonry walls strengthened by vegetal-fabric-reinforced cementitious matrix (FRCM) composites, Eng. Struct. 221 (2020) 111097, https://doi.org/10.1016/j.engstruct.2020.111097.
[13] B. Torres, S. Ivorra, F. Javier Baeza, L. Estevan, B. Varona, Textile reinforced mortars (TRM) for repairing and retrofitting masonry walls subjected to in-plane cyclic loads. An experimental approach, Eng. Struct. 231 (2021) 111742, https://doi.org/10.1016/j.engstruct.2020.111742.
[14] L. Garcia-Ramonda, L. Pelà, P. Roca, G. Camata, Cyclic shear-compression testing of brick masonry walls repaired and retrofitted with basalt textile reinforced mortar, Compos. Struct. 283 (2022), https://doi.org/10.1016/j.compstruct.2021.115068.
[15] P.E. Mezrea, I.A. Yilmaz, M. Ispir, E. Binbir, I.E. Bal, A. Ilki, External jacketing of unreinforced historical masonry piers with open-grid basalt-reinforced mortar, J. Compos. Constr. 21 (2017) 1–16, https://doi.org/10.1061/(asce)cc.1943-5614.0000770.
[16] T. Krevaikas D, Experimental study on carbon fiber textile reinforced mortar system as a means for confinement of masonry columns, Constr. Build. Mater. 208 (2019) 723–733, https://doi.org/10.1016/j.conbuildmat.2019.03.033.
[17] L.N. Koutas, D.A. Bournas, Confinement of masonry columns with textile-reinforced mortar jackets, Constr. Build. Mater. 258 (2020) 120343, https://doi.org/10.1016/j.conbuildmat.2020.120343.
[18] F. Valvona, J. Toti, V. Gattulli, F. Potenza, Effective seismic strengthening and monitoring of a masonry vault by using Glass Fiber Reinforced Cementitious Matrix with embedded Fiber Bragg Grating sensors, Compos. Part B Eng. 113 (2017) 355–370, https://doi.org/10.1016/j.compositesb.2017.01.024.
[19] F.A. Kariou, S.P. Triantafyllou, D.A. Bournas, TRM strengthening of masonry arches: an experimental investigation on the effect of strengthening layout and

textile fibre material, Compos. Part B Eng. 173 (2019) 106765, https://doi.org/10.1016/j.compositesb.2019.04.026.
[20] E. Bertolesi, B. Torres, J.M. Adam, P.A. Calderón, J.J. Moragues, Effectiveness of Textile Reinforced Mortar (TRM) materials for the repair of full-scale timbrel masonry cross vaults, Eng. Struct. 220 (2020) 110978, https://doi.org/10.1016/j.engstruct.2020.110978.
[21] C.C. Papanicolaou, T. Triantafillou, Performance of TRM/TRC systems under elevated temperatures and fire conditions, Am. Concr. Inst., ACI Spec. Publ. (2021) 32–46.
[22] D.A.S. Rambo, F. de Andrade Silva, R.D. Toledo Filho, O. da Fonseca Martins Gomes, Effect of elevated temperatures on the mechanical behavior of basalt textile reinforced refractory concrete, Mater. Des. 65 (2015) 24–33, https://doi.org/10.1016/j.matdes.2014.08.060.
[23] T.H. Nguyen, X.H. Vu, A. Si Larbi, E. Ferrier, Experimental study of the effect of simultaneous mechanical and high-temperature loadings on the behaviour of textile-reinforced concrete (TRC), Constr. Build. Mater. 125 (2016) 253–270, https://doi.org/10.1016/j.conbuildmat.2016.08.026.
[24] L. Estevan, F.B. Varona, F.J. Baeza, B. Torres, D. Bru, Textile reinforced mortars (TRM) tensile behavior after high temperature exposure, Constr. Build. Mater. 328 (2022) 127116, https://doi.org/10.1016/j.conbuildmat.2022.127116.
[25] P. Kapsalis, T. Triantafillou, E. Korda, D. Van Hemelrijck, T. Tysmans, Tensile Performance of textile-reinforced concrete after fire exposure: experimental investigation and analytical approach, J. Compos. Constr. 26 (1) (2022) 23, https://doi.org/10.1061/(asce)cc.1943-5614.0001162.
[26] S.R. Maroudas, C.G. Papanicolaou, Effect of high temperatures on the TRM-to-masonry bond (KEM), Key Eng. Mater. 747 (2017) 533–541, https://doi.org/10.4028/www.scientific.net/KEM.747.533.
[27] A. Iorfida, S. Candamano, F. Crea, L. Ombres, S. Verre, P. De Fazio, Bond behaviour of FRCM composites: effects of high temperature (KEM), Key Eng. Mater. 817 (2019) 161–166, https://doi.org/10.4028/www.scientific.net/KEM.817.161.
[28] P.D. Askouni, C.G. Papanicolaou, L. Azdejkovic, Experimental investigation of the trm-to-masonry bond after exposure to elevated temperatures: cementitious and alkali-activated matrices of various densities, Materials 15 (2022), https://doi.org/10.3390/ma15010140.
[29] L. Estevan, F.J. Baeza, F.B. Varona, J. Pereiro, Effect of high temperature on textile reinforced mortar-to-masonry bond, Constr. Build. Mater. 393 (2023) 132123, https://doi.org/10.1016/j.conbuildmat.2023.132123.
[30] L. Estevan, B. Torres, F.B. Varona, F.J. Baeza, S. Ivorra, Shear strengthening of masonry walls with Textile Reinforced Mortars (TRM) under high temperature exposure, J. Build. Eng. 63 (2023) 105511, https://doi.org/10.1016/j.jobe.2022.105511.
[31] L. Estevan, B. Torres, F.J. Baeza, F.B. Varona, S. Ivorra, Masonry walls strengthened with Textile Reinforced Mortars (TRM) and subjected to in-plane cyclic loads after real fire exposure, Eng. Struct. 296 (2023) 116922, https://doi.org/10.1016/j.engstruct.2023.116922.
[32] N.M. Azmee, N. Shafiq, Ultra-high performance concrete: from fundamental to applications, Case Stud. Constr. Mater. 9 (2018), https://doi.org/10.1016/j.cscm.2018.e00197.
[33] M.A. Bajaber, I.Y. Hakeem, UHPC evolution, development, and utilization in construction: a review, J. Mater. Res. Technol. 10 (2021) 1058–1074, https://doi.org/10.1016/j.jmrt.2020.12.051.
[34] M. Amran, S.S. Huang, A.M. Onaizi, N. Makul, H.S. Abdelgader, T. Ozbakkaloglu, Recent trends in ultra-high performance concrete (UHPC): current status, challenges, and future prospects, Constr. Build. Mater. 352 (2022) 129029, https://doi.org/10.1016/j.conbuildmat.2022.129029.
[35] H. Yin, W. Teo, K. Shirai, Experimental investigation on the behaviour of reinforced concrete slabs strengthened with ultra-high performance concrete, Constr. Build. Mater. 155 (2017) 463–474, https://doi.org/10.1016/j.conbuildmat.2017.08.077.
[36] Y. Zhu, Y. Zhang, H.H. Hussein, G. Chen, Flexural strengthening of reinforced concrete beams or slabs using ultra-high performance concrete (UHPC): a state of the art review, Eng. Struct. 205 (2020) 110035, https://doi.org/10.1016/j.engstruct.2019.110035.
[37] J. Xie, Q. Fu, J.B. Yan, Compressive behaviour of stub concrete column strengthened with ultra-high performance concrete jacket, Constr. Build. Mater. 204 (2019) 643–658, https://doi.org/10.1016/j.conbuildmat.2019.01.220.
[38] J. Donnini, S. Spagnuolo, V. Corinaldesi, A comparison between the use of FRP, FRCM and HPM for concrete confinement, Compos. Part B Eng. 160 (2019) 586–594, https://doi.org/10.1016/j.compositesb.2018.12.111.
[39] V.S. Ronanki, S. Aaleti, Experimental and analytical investigation of UHPC confined concrete behavior, Constr. Build. Mater. 325 (2022) 126710, https://doi.org/10.1016/j.conbuildmat.2022.126710.
[40] B. Peng, S. Wei, L. Long, Q. Zheng, Y. Ma, L. Chen, Experimental investigation on the performance of historical squat masonry walls strengthened by UHPC and reinforced polymer mortar layers, Appl. Sci. 9 (2019), https://doi.org/10.3390/app9102096.
[41] Z. Jiang, J. Yang, H. Su, Mechanical response of masonry structure strengthened with ultra-high performance concrete (UHPC): a comparative analysis for different strengthening tactics, Front. Mater. 10 (2023) 1–24, https://doi.org/10.3389/fmats.2023.1289225.
[42] P. Ganesh, A. Ramachandra Murthy, Simulation of surface preparations to predict the bond behaviour between normal strength concrete and ultra-high performance concrete, Constr. Build. Mater. 250 (2020) 118871, https://doi.org/10.1016/j.conbuildmat.2020.118871.
[43] A. Valikhani, A.J. Jahromi, I.M. Mantawy, A. Azizinamini, Experimental evaluation of concrete-to-UHPC bond strength with correlation to surface roughness for repair application, Constr. Build. Mater. 238 (2020) 117753, https://doi.org/10.1016/j.conbuildmat.2019.117753.
[44] Y. Zhang, P. Zhu, Z. Liao, L. Wang, Interfacial bond properties between normal strength concrete substrate and ultra-high performance concrete as a repair material, Constr. Build. Mater. 235 (2020) 117431, https://doi.org/10.1016/j.conbuildmat.2019.117431.
[45] Z. Zhang, K. Pang, L. Xu, Y. Zou, J. Yang, C. Wang, The bond properties between UHPC and stone under different interface treatment methods, Constr. Build. Mater. 365 (2023) 130092, https://doi.org/10.1016/j.conbuildmat.2022.130092.
[46] G. Choe, G. Kim, N. Gucunski, S. Lee, Evaluation of the mechanical properties of 200 MPa ultra-high-strength concrete at elevated temperatures and residual strength of column, Constr. Build. Mater. 86 (2015) 159–168, https://doi.org/10.1016/j.conbuildmat.2015.03.074.
[47] H. Huang, R. Wang, X. Gao, Improvement effect of fiber alignment on resistance to elevated temperature of ultra-high performance concrete, Compos. Part B Eng. 177 (2019) 107454, https://doi.org/10.1016/j.compositesb.2019.107454.
[48] S. Ahmad, M. Rasul, S.K. Adekunle, S.U. Al-Dulaijan, M. Maslehuddin, S.I. Ali, Mechanical properties of steel fiber-reinforced UHPC mixtures exposed to elevated temperature: effects of exposure duration and fiber content, Compos. Part B Eng. 168 (2019) 291–301, https://doi.org/10.1016/j.compositesb.2018.12.083.
[49] G.D. Ashkezari, M. Razmara, Thermal and mechanical evaluation of ultra-high performance fiber-reinforced concrete and conventional concrete subjected to high temperatures, J. Build. Eng. 32 (2020) 101621, https://doi.org/10.1016/j.jobe.2020.101621.
[50] Y. Zhu, H. Hussein, A. Kumar, G. Chen, A review: material and structural properties of UHPC at elevated temperatures or fire conditions, Cem. Concr. Compos. 123 (2021) 104212, https://doi.org/10.1016/j.cemconcomp.2021.104212.
[51] F. Sciarretta, S. Fava, M. Francini, L. Ponticelli, M. Caciolai, B. Briseghella, C. Nuti, Research on the high temperature behaviour of ultra-high-performance concrete (UHPC) with polypropylene (PP) and steel fibres (LNCE), Lect. Notes Civ. Eng. 435 (2024) 681–693, https://doi.org/10.1007/978-3-031-43102-9_52.
[52] ACI 549.6R-20, Guide to Design and Construction of Externally Bonded Fabric-Reinforced Cementitious Matrix and Steel-Reinforced Grout Systems for Repair and Strengthening of Concrete Structures, American Concrete Institute, ACI Committee 549 (2020).
[53] CNR-DT 215/2018, Guide for the Design and Construction of Externally Bonded Fibre Reinforced Inorganic Matrix Systems for Strengthening Existing Structures, CNR - Advisory Committee on Technical Recommendations for Construction, Rome, Italy (2020).
[54] EN 1504–3:2005, Products and systems for the protection and repair of concrete structures – Definitions, requirements, quality control and evaluation of conformity – Part 3: Structural and non-structural repair, European Committee for Standardization, Brussel (2005).
[55] EN 1015–11:2019, Methods of test for mortar for masonry – Part 11: Determination of flexural and compressive strength of hardened mortar, European Committee for Standardization, Brussels (2019).
[56] AC434, Acceptance Criteria for Masonry and Concrete Strengthening Using Fiber-Reinforced Cementitious Matrix (FRCM) and Steel Reinforced Grout (SRG) Composite Systems, ICC Evaluation Service (2018).
[57] RILEM Technical Committee 232-TDT (Wolfgang Brameshuber), Recommendation of RILEM TC 232-TDT: test methods and design of textile reinforced concrete. Uniaxial tensile test: test method to determine the load bearing behavior of tensile specimens made of textile reinforced concrete, Mater. Struct. 49 (2016) 4923–4927, https://doi.org/10.1617/s11527-016-0839-z.
[58] ASTM D2845–08. Standard Test Method for Laboratory Determination of Pulse Velocities and Ultrasonic Elastic Constants of Rock, ASTM International, West Conshohocken, PA, 2008.
[59] ASTM E1875–20a. Standard Test Method for Dynamic Young's Modulus, Shear Modulus, and Poisson's Ratio by Sonic Resonance, ASTM International, West Conshohocken, PA, 2020.
[60] EN 1052–3:2002, Methods of test for masonry – Part 3: Determination of initial shear strength, European Committee for Standardization, Brussels (2002).
[61] B. Torres, F.B. Varona, F.J. Baeza, D. Bru, S. Ivorra, Study on retrofitted masonry elements under shear using digital image correlation, Sensors 20 (2020), https://doi.org/10.3390/s20072122.
[62] E. Bertolesi, M. Fagone, T. Rotunno, E. Grande, G. Milani, Experimental characterization of the textile-to-mortar bond through distributed optical sensors, Constr. Build. Mater. 326 (2022) 126640, https://doi.org/10.1016/j.conbuildmat.2022.126640.
[63] EN 1996–1–1:2005+A1:2012, Eurocode 6: Design of masonry structures – Part 1–1: General rules for reinforced and unreinforced masonry structures, European Committee for Standardization, Brussels (2012).
[64] ASTM E519/E519M–21. Standard Test Method for Diagonal Tension (Shear) in Masonry Assemblages, ASTM International, West Conshohocken, PA, 2021.